CHAPTER VI

A SIMPLE ROOM TEMPERATURE SYNTHESIS OF Fe-SBA-15 FROM SILATRANE AND $FeCl_3$ VIA SOL-GEL PROCESS AND ITS CATALYTIC PROPERTIES IN EPOXIDATION OF STYRENE WITH H_2O_2

6.1 Abstract

Functionalized Fe-SBA-15 mesoporous silica catalysts with *p6mm* symmetry have been synthesized through a simple room temperature sol-gel process from moisture resistant silatrane and $FeCl_3$ as silicon and iron sources, and a non-ionic triblock copolymer ($EO_{20}PO_{70}EO_{20}$) as the structure directing agent. Small angle X-ray scattering (SAXS), transmission electron microscopy (TEM) and field emission scanning electron microscopy (FESEM) showed well-ordered 2D mesoporous hexagonal structures. The incorporation of ferric ion into the SBA-15 framework was investigated by diffuse reflectance UV-visible spectroscopy (DRUV) that confirmed tetrahedral coordination (FeO_4) is maintained to a loading of 10% mol Fe. N_2 adsorption/desorption measurements yielded high surface areas (up to 715 m^2/g), with large pore diameters (5.4 nm) and volumes (0.93 cm^3/g). The catalytic activity of Fe-SBA-15 was evaluated by epoxidation of styrene monomer with hydrogen peroxide (H_2O_2), to achieve a higher styrene conversion (10.3%) than a benchmark material synthesized by impregnation (7.2%). The sol-gel catalyst produces styrene oxide and benzaldehyde with selectivity of 34.5% and 65.5%, while the impregnated catalyst delivers benzaldehyde only under identical reaction conditions.

(**Keywords**: Fe-SBA-15, silatrane, sol-gel process, styrene epoxidation)

6.2 Introduction

Since the discovery of well-ordered, large diameter (4.6–30 nm) mesoporous silica SBA-15 with a uniform hexagonal structure, high specific surface area, and excellent hydrothermal stability [1, 2], considerable effort has been devoted

towards the functionalization of these materials as catalysts, absorbents, chemical sensors and nanodevices among many possible applications. The incorporation of metals into zeolite frameworks or the walls of mesoporous silica create Brønsted acid sites whose concentration can be tuned to optimize catalytic and absorptive properties [3-6]. Specifically, iron(III)-substituted mesoporous silica shows excellent redox properties and high activity in alkylation and oxidation reactions [7-10]. However, the incorporation of metal ions into SBA-15 is not straightforward because the strongly acidic conditions (pH <2) favor dissolution of the dopant species. Several studies have dealt with "incorporation" of metals in SBA-15 using post-synthesis methods, however, it is not always clear if the association is crystallographic or by surface decoration. Therefore, direct syntheses are often preferred to minimize the number of processing steps and generate uniform mesopore arrays and high loadings of metal without channel blocking. Fe-SBA-15 is usually synthesized hydrothermally (100 °C/48 h) by employing tetraethylorthosilicate as the silica source, but this approach can suffer from significant alkoxide hydrolysis. Commercially available silica sources are highly susceptible to hydrolysis, resulting in the rapid separation of amorphous silica that impedes mesopore formation. Therefore, this work was undertaken to prepare Fe-SBA-15 using moisture resistant silatrane [11] where the reaction proceeds at room temperature rather than hydrothermally treatment. Silatrane has been demonstrated as an effective precursor for many technological materials [12-16] and proven successful for the synthesis of SBA-15 under ambient conditions [17]. Recently, Samran et al. [17] described the use of silatrane for the direct crystallochemical incorporation of Ti^{4+} (7 mol% Ti) into the SBA-15 framework by displacement of Si^{4+}. Here, we extend this synthetic methodology to the preparation of mesoporous ferrisilicate Fe-SBA-15 with a focus on iron speciation, location of the dopant and catalytic activity. The primary tools include small angle X-ray scattering (SAXS), transmission electron microscopy (TEM), field emission scanning electron microscopy (FESEM), diffuse reflectance UV-visible spectroscopy (DRUV), and N_2 adsorption. The catalytic response was investigated via epoxidation of styrene monomer with H_2O_2 employed as the oxidant, as a function of temperature, time,

catalyst loading, Fe content and styrene:H_2O_2 ratio. For benchmarking, catalytic performance was compared for materials synthesized via sol-gel (Si^{4+} displacement by Fe^{3+}) and impregnation (deposition of Fe_2O_3) methods.

6.3 Experimental

6.3.1 Materials

Fumed silica (SiO_2, 99.8%) (Sigma-Aldrich, St. Louis, MO), triethanolamine (TEA) (Carlo Erba, Milan, Italy), ethylene glycol (EG) (J.T. Baker, Philipsburg, NJ), acetronitrile (Labscan, Bangkok, Thailand), ferric chloride ($FeCl_3$) (Sigma-Aldrich, St. Louis, MO), poly(ethylene glycol)-block-poly(propylene glycol)-block-poly(ethylene glycol) ($EO_{20}PO_{70}EO_{20}$) (Sigma-Aldrich, Singapore), hydrochloric acid (HCl) (Labscan, Asia), hydrogen peroxide (H_2O_2) (Labscan, Asia), and styrene monomer (Labscan, Asia) were used without further treatment.

6.3.2 Fe-SBA-15 sol-gel synthesis

Fe-SBA-15 was synthesized from silatrane and $FeCl_3$ as the silica and iron sources, respectively. The non-ionic triblock copolymer surfactant $EO_{20}PO_{70}EO_{20}$ was used as the structure-directing agent and 2 M HCl was the acid catalyst. The preparation of Fe-SBA-15 with different n_{Fe}/n_{Si} molar ratios followed the method of Samran *et al.* [17]. A solution of $EO_{20}PO_{70}EO_{20}$:HCl:silatrane:H_2O = 2:60:4.25:12 (mass ratio) was prepared by dissolving 4 g of $EO_{20}PO_{70}EO_{20}$ polymer in 80 g of 2 M HCl (part A) and 8.8 g of silatrane [18, 19], in 20 g of H_2O (part B) with continuous stirring for 1 h to ensure complete dissolution. The solution of part B was then poured into part A. The required amount of $FeCl_3$ was added to the homogenous solution with stirring. The resulting gel was aged at room temperature (RT) for 24 h and the product recovered by filtration, washed with deionized water, and dried at ambient overnight. This resin was calcined (550 °C/air/6 h) in a tube furnace (Carbolite, CFS 1200, Hope Valley, U.K.) at a heating rate of 0.5 °C/min to remove residual organics. The catalysts were designated as *(x)* mol% Fe-SBA-15 where x denotes the n_{Fe}/n_{Si} percentage used during synthesis. Iron-free SBA-15 was

synthesized using the same procedure ($EO_{20}PO_{70}EO_{20}$:HCl:silatrane:H_2O = 2:60:4.25:12) in the absence of $FeCl_3$.

6.3.3 Impregnation synthesis

Fe-SBA-15 was also prepared by incipient wetness impregnation [20] by dropping an $FeCl_3$ solution (40 mg/ml) onto SBA-15 followed by oven drying (100 °C/12 h) and air calcination (550 °C/6 h) in a carbolite tube furnace (CFS 1200) at a heating rate of 0.5 °C/min.

6.3.4 Characterization

The products were characterized by powder X-ray diffraction with a PANalytical PW3830 instrument using CuKα (λ_{av} = 0.154 nm) radiation generated at 50kV and 40 mA, over the 2θ range 0.5–10°, step size of 0.01° and dwell time of 10 seconds per step. Transmission electron microscopy (TEM) was conducted using a Hitachi H-7100FA machine operating at 125 kV with a large objective aperture. Field emission scanning electron microscopy (FESEM) was used to collect secondary electron images from powders mounted on double-sided carbon tape using a Zeiss Ultra plus, operating at 0.3–0.5 kV to minimize charging. Nitrogen adsoption and desorption isotherms were measured at -196 °C after outgassing at 250 °C for 12 h under vacuum (Quantasorb JR, Mount Holly, NJ) to determine the Brunauer–Emmett–Teller (BET) specific surface area. The pore size distributions were obtained from the adsorption and desorption branches of the nitrogen isotherms by the Barrett-Joyner-Halenda method. Diffuse reflectance UV-visible (DRUV) spectroscopic measurements were recorded on a Shimadzu UV-2550 spectrophotometer fitted with an ISR-2200 integrating sphere attachment and recorded from 190–600 nm and using $BaSO_4$ as a reference.

6.3.5 Catalytic activity

The epoxidation of styrene was measured from data collected in a batch reactor. The catalyst (0.05–0.15 g), styrene (5 mmol), hydrogen peroxide (5–15 mmol of 30 wt% aqueous solution) and acetronitrile (5 ml) were introduced to a glass flask with closed cap (30 ml). The reactant mixture was stirred and heated for a fixed time (8–24 h) and temperature (50–80 °C) in an oil bath. The products were identified and quantified by gas chromatography (GC) employing a capillary column

(DB-Wax, 30 m x 0.25 mm) and flame ionization detector (FID). The conversion of styrene was calculated based upon the quantity of styrene monomer consumed.

6.4 Results and Discussion

6.4.1 Mesostructure and Crystal Chemistry

Zhao *et al.* [1] synthesized good quality SBA-15 of high surface area (690 m^2/g) from aged TEOS (35 °C/20 h) prior to hydrothermal reaction (100 °C/48 h). Recently, Samran *et al.* [17] reported a novel method to prepare SBA-15 from silatrane at room temperature via a sol-gel process using a nonionic triblock copolymer as the template to avoid the need for hydrothermal treatment. Following this approach, high quality Ti-SBA-15, of large surface area (592–670 m^2/g), pore volume (0.83 cm^3/g) and pore size (5.7 nm), was readily obtained. This synthetic methodology was extended to the present study for preparation of mesoporous ferrisilicate Fe-SBA-15.

SAXS of pure siliceous SBA-15 and Fe-SBA-15 with nominal loadings of 1-20 mol% Fe after calcination, show the expected patterns [17] with {10} ≡ {11} and {30} ≡ {33} reflections consistent with *p6mm* plane symmetry at 2θ 0.45° and 1.35° (Figure 1). This hexagonal motif was observed for all Fe-SBA-15 indicating that mesopore order in SBA-15 was sustained after the introduction of iron into the framework, due to the mild synthesis conditions and extraordinarily high purity and moisture resistance of the silatrane precursor. The hexagonal translational parameter (a_0) calculated from $a_0 = 2d(100)/\sqrt{3}$, increased with Fe content consistent with incorporation of Fe in the framework; the dilation may arise (at least partly) because the ionic radius of Fe^{3+} is larger than Si^{4+} (r^{3+}_{Fe} = 0.63 Å and r^{4+}_{Si} = 0.40 Å), indicative of $Si^{4+} + O^{2-} \leftrightarrow Fe^{3+} + OH^-$ substitution. As a_0 does not increase for Fe content > 10 mol% an upper limit for framework incorporation is supposed under these synthetic conditions [8, 21]. The shift of d-spacings to smaller angles with increasing in Fe loading is analogous to other metal-substituted mesoporous materials [10]. FESEM of 10 mol% Fe-SBA-15 calcine (Figure 2) yielded secondary electron images that exhibit the typical hexagonal rod-like morphology of SBA-15.

Bright field transmission electron micrographs (Figure 3) show aligned channels, confirming a long range hexagonal structure Fe-SBA-15.

The porosity of Fe-SBA-15 samples measured by N_2 adsorption at 77K all yield type IV isotherms (IUPAC classification) and exhibit broad H1 type hysteresis loops, typical of large-pore mesoporous solids (Figure 4). The well-defined step at a relatively high pressure of 0.5–0.7 corresponds to capillary condensation of N_2 within uniform pores (> 5 nm diameter) and high surface area (up to 751 m^2/g) (Table 1). All the materials exhibited large surface areas (588–751 m^2/g) and pore volumes (0.69–0.93 cm^3/g) with a narrow pore size distribution (1.5–1.9 nm). The incorporation of Fe into the framework of SBA-15 was beneficial with the BET surface area, pore volume and pore diameter all improving with iron incorporation. Pore diameter dilation with increasing Fe content is consistent with SAXS, and is attributed to the silatrane route minimizing pore blockage by Fe_2O_3.

DRUV spectroscopy of the calcined Fe-SBA-15 with 2.5–20 mol% Fe all yielded Fe/Si mole ratioes lower than 10 mol% Fe with respect to the strong adsorption band at 210–250 nm, although the intensity increased with Fe loading to this limit (Figure 5). This band can be assigned to dπ-pπ charge transfer between the Fe and O across framework Fe-O-Si bridging bonds [22], and is associated with ligand-to-metal charge transfer in isolated 4-coordinated Fe^{3+}. When the nominal Fe/Si molar ratio was < 15 mol%, there was no significant adsorption at 320 nm that would be consistent with iron oligomer or aggregated Fe_2O_3 clusters [4]. However, this adsorption band did appear at higher level and became more obvious at 20 mol% which is indicative of extra-framework iron. These results provide further evidence that the upper limit of framework iron incorporation in SBA-15 is less than 15 mol% Fe.

6.4.2 Catalytic activity

Catalytic activity was tested via the epoxidation of styrene monomer in a batch-type reactor using H_2O_2 as an oxidant. At the end of the reaction the catalyst was filtered and the products analyzed by gas chromatography (Table 2); a blank reaction performed over pure SBA-15 under identical conditions showed no catalytic activity. Hydrogen peroxide alone was also unable to oxidize styrene in the

absence of mesoporous silica, whereas all Fe-SBA-15 samples were efficient catalysts. The only products are minor styrene oxide and major benzaldehyde, with the conversion of styrene increasing from 2.9% to 10.3% in passing from 1 mol% Fe to 10 mol% Fe. At this upper iron content, the conversion of styrene is maximal with selectivities of styrene oxide and benzaldehyde being 34.5 and 65.5%, respectively, beyond which conversion efficiency decreased. This result is consistent with DRUV, demonstrating that the active metal sites are incorporated in the framework [4], as confirmed by the absence of reactivity of pure SBA-15. It is reasonable to conclude that isolated tetrahedrally coordinated iron is responsible for the oxidation of styrene [23]. Additionally, Fe-SBA-15 prepared by the sol-gel synthesis method showed relatively higher conversion of styrene (10.3%) than an equivalent catalyst (in terms of Fe content) synthesized by the impregnation method (7.2%), where poor dispersion and mesopore plugs of metal oxides appear responsible for relatively poor catalytic activity [24]. Interestingly, benzaldehyde is the only product obtained from the catalyst prepared by the impregnation method, an outcome that might arise either because: (i) benzaldehyde is produced during nucleophilic attack of H_2O_2 to styrene oxide followed by a cleavage of the intermediate hydroxyl-hydroperoxistyrene (Scheme 1, route B), or (ii) benzaldehyde results from a radical mechanism through direct oxidative cleavage of the styrene side chain double bond (Scheme 1, route C) [25].

The styrene conversion was unchanged when the mole ratios of styrene: H_2O_2 are 1:1 or 1:2 (Table 3). The highest styrene conversion (20.3%) was obtained at a ratio of 1:3, but with benzaldehyde as sole product. Although excess H_2O_2 accelerates styrene conversion it also causes the secondary oxidation of the epoxide and the formation of benzaldehyde through the cleavage of the C=C bond [23, 25]. With increasing catalyst mass (0.05 g to 0.15 g) styrene conversion slightly increases from 10.3% to 12.6% and selectivities of styrene oxide and benzaldehyde are 65.5 to 71.2% and 34.5 to 28.8%, respectively (Table 4). While the styrene conversion rate was essentially constant, the slight enhancement with increasing catalyst mass could reflect an increase in the number of active Fe sites available for oxidization [26, 27]. As expected, when the reaction temperature was raised (50° - 80

°C), the conversion rate increases and selectivity of styrene oxide is 37.9% at 50 °C, but slightly decreases at higher temperature (Table 5). In contrast, the selectivity of benzaldehyde increased slightly at the cost of the styrene oxide, indicating that benzaldehyde is formed mainly via further oxidation of styrene oxide, and that the higher temperature favors the oxidation of styrene oxide (Scheme 1, route B). This result accords with Zhang et al. [23] and Li et al. [24]. Table 6 shows that styrene conversion as a function of reaction time at 70 °C increases chronologically while styrene oxide selectivity decreases. However, over time a slight decrease in styrene oxidation is noticed with a corresponding increase in benzaldehyde selectivity; this can be attributed to secondary oxidation of epoxide [23].

6.5 Conclusions

Fe-SBA-15 was successfully synthesized via a sol-gel process using silatrane as the silica precursor, ferric chloride as the iron source, and a nonionic triblock copolymer ($EO_{20}PO_{70}EO_{20}$) as template. This room temperature synthesis is simple and avoids hydrothermal treatment as conventionally required. The catalysts maintained a *p6mm* hexagonal mesostructure, high surface area (715 m^2/g), large pore diameter (5.40 nm) and volume (0.93 cm^3/g). The optimal ferric ion (FeO_4) framework loading of SBA-15, without separation of extra-framework Fe_2O_3, is 10 mol% Fe. In addition, these Fe-SBA-15 materials show high catalytic activity towards the epoxidation of styrene monomer with hydrogen peroxide due to the presence of active iron species in the SBA-15 framework. The product obtained from sol-gel synthesis method provides superior catalytic activity compared to the impregnation method. The optimal condition for epoxidation of styrene over Fe-SBA-15 is 70 °C for 24 h, using 0.05 g catalyst containing 10 mol% of iron content, and a 1:1 mol ratio of styrene:H_2O_2. The only products obtained are styrene oxide and benzaldehyde. The selectivity of styrene oxide and benzaldehyde reached 34.5% and 65.5% at a styrene conversion of 10.3%, and demonstrates that Fe-SBA-15 heterocatalyst can be synthesized by an inexpensive and energy saving process for a range of catalytic applications.

6.6 Acknowledgements

This research work is financially supported by the Postgraduate Education and Research Program in Petroleum and Petrochemical Technology (ADB) Fund (Thailand), and the Ratchadapisake Sompote Fund, Chulalongkorn University. The SAXS patterns were collected by Mr. An Tao and Ms. Li Henan at the School of Materials Science and Engineering, Nanyang Technological University. Dr. Frank Brink of the Australian National University collected the secondary electron images.

6.7 References

1. Zhao, D.; Feng, J.; Huo, Q.; Melosh, N.; Frerickson, G. H.; Chmelka, B. F.; Stucky, G. D. *Science* **1998**, *279*, 548-552.
2. Zhao, D.; Huo, Q.; Feng, J.; Chmelka, B. F.; Stucky, G. D. *J. Am. Chem. Soc.* **1998**, *120*, 6024-6036.
3. He, N.; Bao, S.; Xu, Q. *Appl. Catal., A* **1998**, *169*, 29.
4. Tuel, A.; Acron, I.; Millet, J. M. M. *J. Chem. Soc., Faraday Trans.* B **1998**, *94*, 3501.
5. Corma, A.; Fornes, V.; Navarro, M. T.; Perez-Pariente, J. *J. Catal.* **1994**, *148*, 569.
6. Vinu, A.; Murugesan, V.; Bohlmann, W.; Hartmann, M. *J. Phys. Chem. B.* **2004**, *108*, 11496.
7. Zhang, Y.; Gao, F.; Wan, H.; Wu, C.; Kong, Y.; Wu, X.; Zhao, B.; Dong, L.; Chen, Y. *Micropor. Mesopor. Mater.* **2008**, *113*, 393–401.
8. Vinu, A.; Sawant, D. P.; Ariga, K.; Hossain, K. Z.; Halligudi, S. B.; Hartmann M.; Nomura, M. *Chem. Mater.* **2005**, *17*, 5339-5345.
9. Li, Y.; Feng, Z.; Lian, Y.; Sun, K.; Zhang, L.; Jia, G.; Yang, Q.; Li, C. *Micropor. Mesopor. Mater.* **2005**, *84*, 41-49.
10. Lui, C.; Chen, C.; Leu, J.; Lin, Y. *J. Sol-Gel Sci Techn* **2007**, *43*, 47-51.
11. Piboonchaisit P.; Wongkasemjit S.; Laine R. *J. Sci. Soc. Thailand* **1999**, *25*, 113.
12. Phonthammachai, N.; Chairassameewong, T.; Gulari, E.; Jemieson, A.M.; Wongksemjit, S. *Microporous and Mesoporous Material* **2003**, *66*, 261-271.

13. Tanglumlert, W.; Imae, T.; White, T. J.; Wongkasemjit, S. *Materials Letters* **2008**, *62*, 4545-4548.
14. Sathupanya, M.; Gulari, E.; Wongkasemjit, S. *J. Eur. Ceram. Soc.* **2003**, *23*, 2305–2314.
15. Phiriyawirut, P.; Jamieson, A. M.; Wongkasemjit, S. *Microporous Mesoporous Mater.* **2005**, *77*, 203–213.
16. Thanabodeekij, N.; Sadthayanon, S.; Gulari, E.; Wongkasemjit, S. *Mater. Chem. Phys.* **2006**, *98*, 131–137.
17. Samran, B.; White, T.J.; Wongkasemjit, S. *Journal of Porous Materials* **2010** DOI. 10.1007/s10934-010-9367-3
18. Phiriyawirut, P.; Magaraphan, R.; Jamieson, A. M.; Wongkasemjit, S. *Material Science and Engineering A* **2003**, *361*, 147-154.
19. Charoenpinijkarn, W.; Suwankruhasn, M.; Kesapabutr, B.; Wongkasemjit, S.; Jamieson, A. M. *European Polymer Journal* **2001**, *37*, 1441-1448.
20. Tanglumlert, W.; Imae, T.; White, T. J.; Wongkasemjit, S. *Cat. Comm.* **2009**, *10*, 1070-1073.
21. Cheng, C. F.; Klinowski, J. *J. Chem. Soc., Faraday trans. B.* **1996**, *92*, 289.
22. Wang, Y.; Zhang, Q.; Shishido, T.; Takehira, K. *J. Catal.* **2002**, *209*,186-196.
23. Ji, D.; Zhao, R.; Lv, G.; Qian, G.; Yan, L.; Suo, J. *Applied Catalysis A : General* **2005**, *281*, 39-45
24. Zhang, L.; Hua, Z.; Dong X.; Li, L.; Chen, H.; Shi, J. *Journal of molecular catalysis A: Chemical* **2007**, *268*, 155-162.
25. Hulea, V.; Dumitriu, E. *Applied Catalysis A : General* **2004**, *277*, 99-106.
26. Wongkasemjit, S.; Tamuang, S.; Tanglumlert, W.; Imae, T. *Materials Chemistry and Physics* **2009**, *117*, 301-306.
27. Tanglumlert, W.; Imae, T.; White, T.J.; Wongkasemjit, S. *J. Am. Ceram. Soc.* **2007**, *90*, 3992-3997.

Table 1. Physical and crystallographic properties of Fe-SBA-15 samples as a function of Fe loading

Sample	Physical properties				Crystallographic properties	
Loaded Fe (%)	Surface area (m^2/g)	Pore Volume (cm^3/g)	Channel diameter (nm)		d_{10}(nm)	a_0(nm)
	BET	BET	BET	SAXS	SAXS	SAXS
Pure SBA-15	570	0.72	5.03	6.0-6.3	18.2	21.0
1.0	588	0.69	5.02	5.9-6.2	18.5	21.3
2.5	751	0.73	5.03	6.4-6.7	18.5	21.3
5.0	710	0.93	5.04	6.2-6.5	18.5	21.3
7.5	715	0.73	5.37	6.3-6.6	19.5	22.5
10.0	601	0.76	5.34	6.2-6.5	18.5	21.3
15.0	637	0.76	5.40	-	-	-
20.0	667	0.70	5.39	6.3-6.6	18.2	21.0

Table 2. Epoxidation of styrene monomer with H_2O_2 over Fe-SBA-15 as a function of Fe loading

Loaded Fe (mol %)	Styrene conversion (%)	Selectivity (%)	
		Benzaldehyde	Styrene oxide
Styrene and H_2O_2*	-	-	-
Pure SBA-15	-	-	-
0.025% Fe	2.9	71.9	28.1
0.050% Fe	6.6	86.1	13.9
0.075% Fe	6.9	72.4	27.6
0.10% Fe	10.3	65.5	34.5
0.15% Fe	5.3	82.2	17.8
0.20% Fe	8.6	46.8	53.2
0.10% Fe (impreg.)	7.2	>99	-
0.20% Fe (impreg.)	8.2	>99	-

*The reaction was conducted in the absence of mesoporous silica.
Reaction condition: catalyst 0.05 g/70 °C/24 h/styrene:H_2O_2 = 1:1

Table 3. Epoxidation of styrene monomer with H_2O_2 over Fe-SBA-15 as a function of mole ratio of styrene:H_2O_2

Mole ratio of styrene:H_2O_2	Styrene conversion (%)	Selectivity (%)	
		Benzaldehyde	Styrene oxide
1:1	10.3	65.5	34.5
1:2	10.8	68.5	31.5
1:3	20.8	>99	-

Reaction condition: 0.05 g of 10 mol% Fe/70 °C/24 h

Table 4. Epoxidation of styrene monomer with H_2O_2 over Fe-SBA-15 as a function of catalyst used

Catalyst used (g)	Styrene conversion (%)	Selectivity (%)	
		Benzaldehyde	Styrene oxide
0.05	10.3	65.5	34.5
0.10	12.6	61.4	38.6
0.15	12.5	71.2	28.8

Reaction condition: 10 mol% Fe/70 °C/24 h/styrene:H_2O_2 = 1:1

Table 5. Epoxidation of styrene monomer with H_2O_2 over Fe-SBA-15 as a function of reaction temperature

Temperature (°C)	Styrene conversion (%)	Selectivity (%)	
		Benzaldehyde	Styrene oxide
50	8.3	63.1	37.9
60	8.5	63.0	37.0
70	10.3	65.5	34.5
80	10.5	70.7	29.3

Reaction condition: 0.05 g of 10 mol% Fe/styrene:H_2O_2 = 1:1

Table 6. Epoxidation of styrene monomer with H_2O_2 over Fe-SBA-15 as a function of reaction time

Time (h)	Styrene conversion (%)	Selectivity (%)	
		Benzaldehyde	Styrene oxide
8	2.8	62.2	37.8
16	6.7	65.4	34.6
24	10.3	65.5	34.5

Reaction condition: 0.05 g of 10 mol% Fe/styrene:H_2O_2 = 1:1

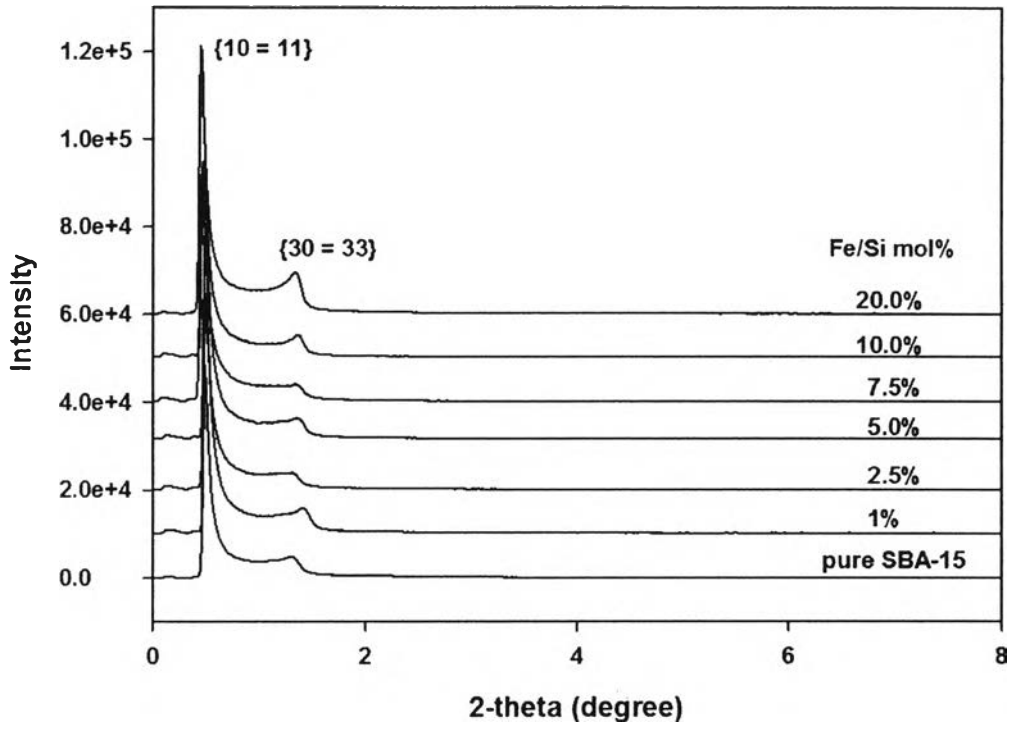

Figure 1 SAXS patterns of pure silica SBA-15 and Fe-SBA-15 containing different amount of Fe loadings

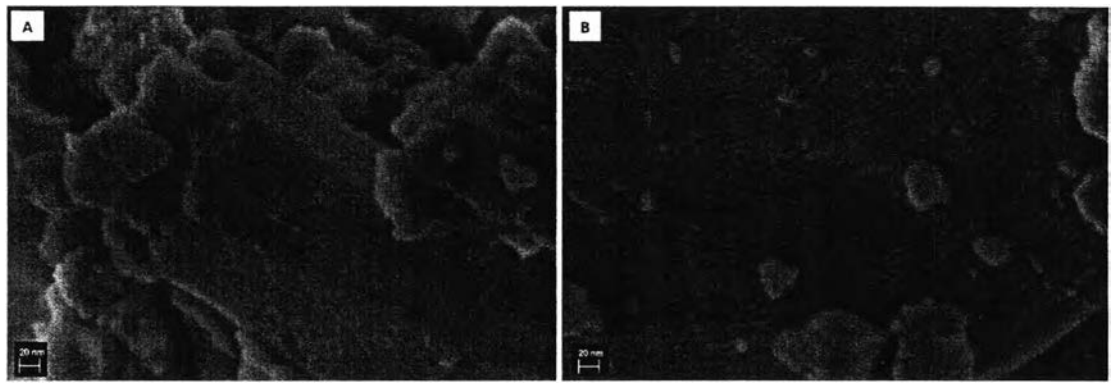

Figure 2 FESEM images of Fe-SBA-15 containing 10 mol% Fe when (A) viewed along the pseudo-hexagonal projection and (B) in the direction parallel to the pore axis

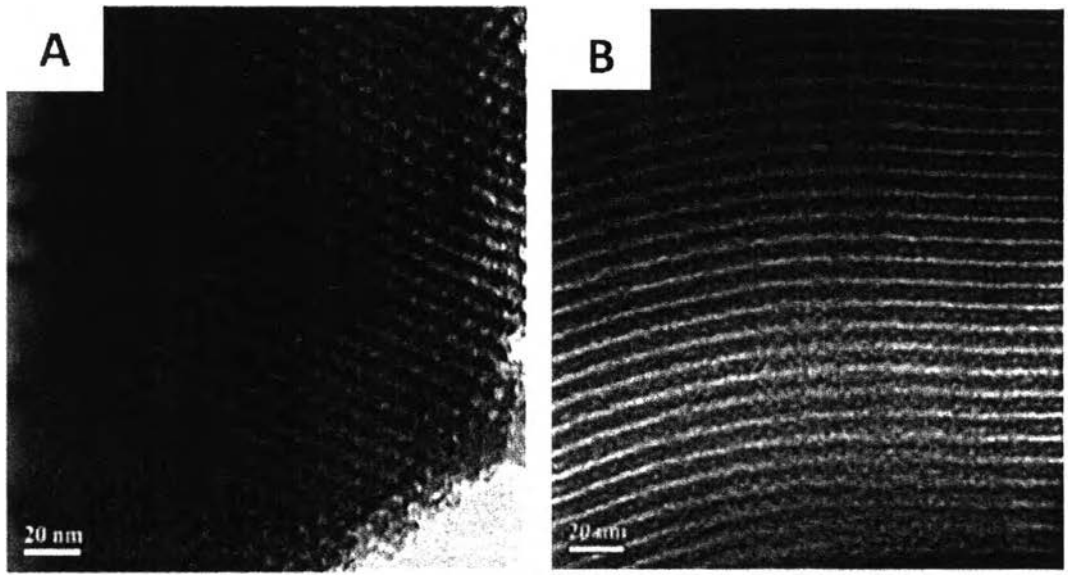

Figure 3 TEM images of Fe-SBA-15 containing 10 mol% Fe (A) in the direction perpendicular to the pore axis and (B) in the direction parallel to the pore axis

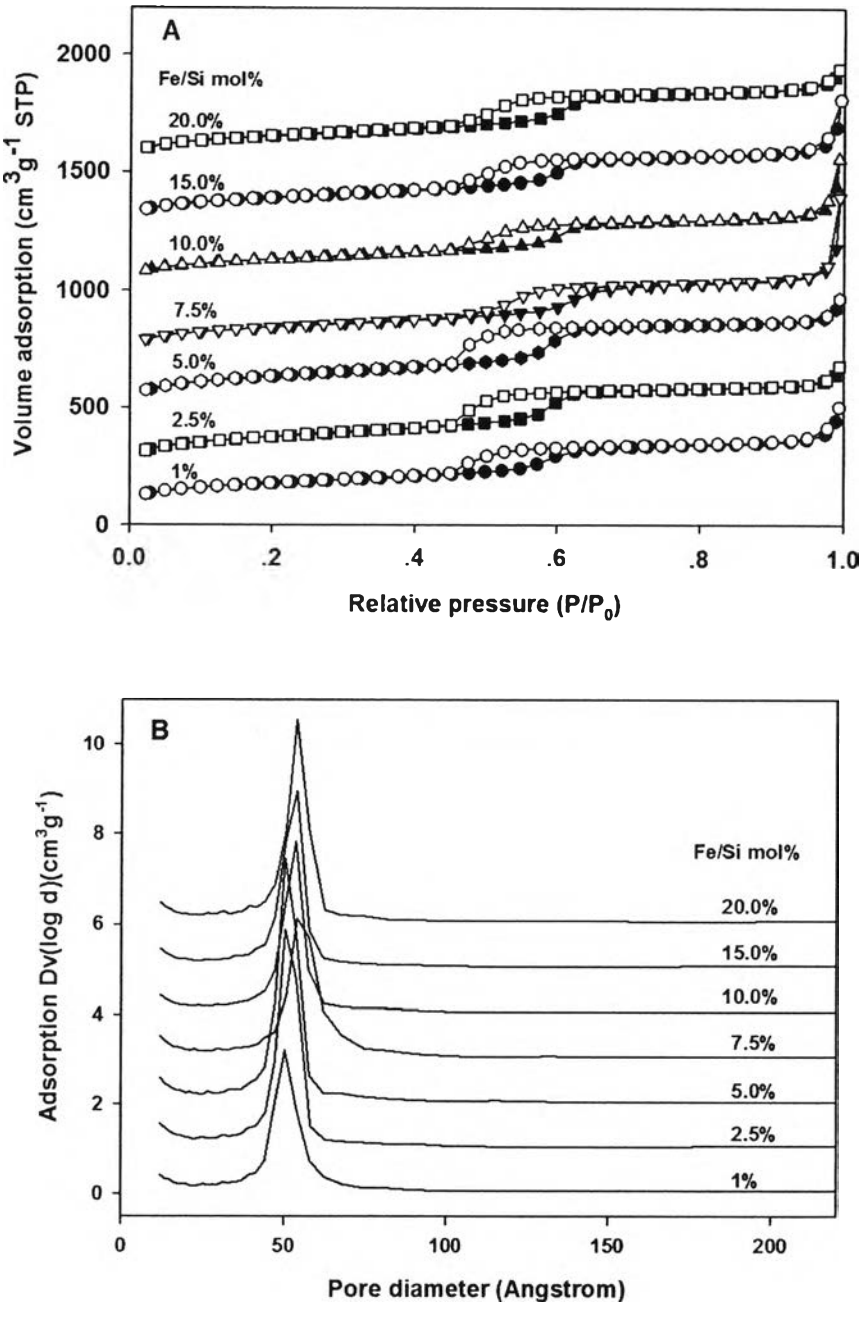

Figure 4 N_2 adsorption/desorption isotherms (A) and pore size distributions (B) of Fe-SBA-15

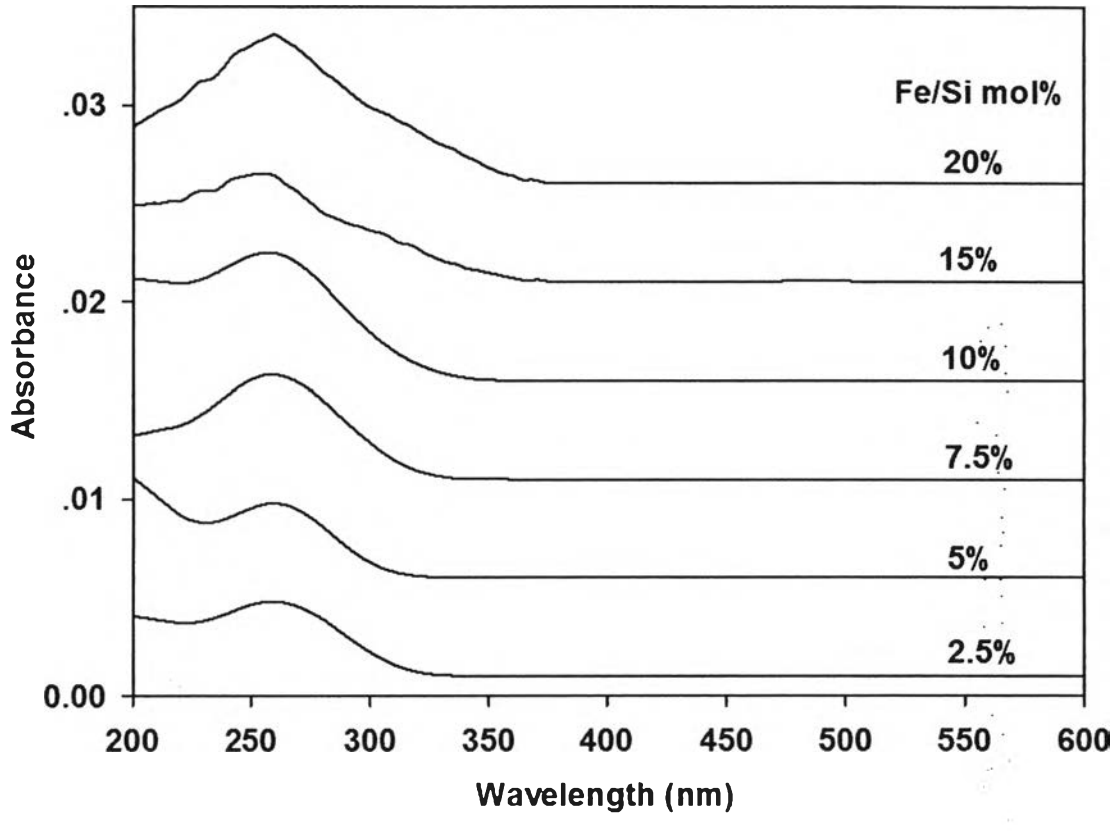

Figure 5 Diffuse reflectance UV-visible spectra of the synthesized Fe-SBA-15

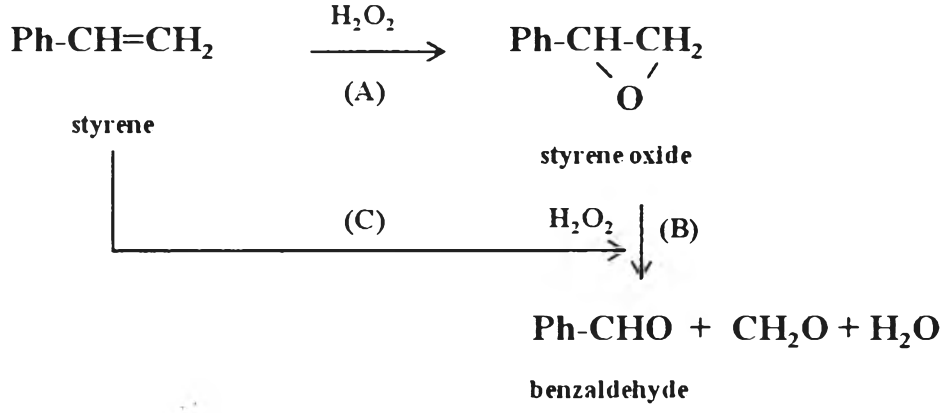
Ph-CH=CH2
H2O2
(A)
Ph-CH-CH2
O
styrene
styrene oxide
(C)
H2O2
(B)
Ph-CHO + CH2O + H2O
benzaldehyde

Scheme 1.